SLAC-PUB-95-6783
LBL-36943

Study of photosensitive mixtures of TMAE and helium, hydrocarbon or CF_4-based carrier gases.

J. Va'vra
Stanford Linear Accelerator Center, Stanford University,
Stanford, CA 94309, U.S.A.

J. Kadyk and J. Wise*
Lawrence Berkeley Laboratory, University of California,
Berkeley, CA 94720, U.S.A.

P. Coyle
Centre de Physique des Particules, Faculte des Sciences de Luminy
CNRS, 13288 Marseille, France

ABSTRACT

Among the photocathodes used for particle identification based on the Cherenkov Ring Imaging technique, the TMAE molecule is still the best in terms of quantum efficiency. Despite the fact that TMAE gaseous photocathodes have already been used in a number of large experiments, one still seeks answers to many detailed questions. We present a systematic study of gaseous photocathodes based on TMAE mixed with helium, hydrocarbon and CF_4-based gases at normal pressure. The study includes a measurement of the electron drift velocity, gas quenching properties, single electron pulse height spectra and anode wire aging. The paper makes recommendations for carrier gas mixtures to obtain the best quenching, and suggests how to manage TMAE wire aging. This study was motivated by a specific particle identification detector proposal, the Fast Drift CRID proposed for the B-factory at SLAC.

Submitted to Nuclear Instruments and Methods

The work was supported by the Department of Energy contract DE-AC03765SF00515.

* Present address : Sandia National Labs, P.O. Box 5800, Albuquerque, NM 87185, U.S.A.

1. INTRODUCTION.

Among the photocathodes used for particle identification based on the Cherenkov Ring Imaging technique [1], TMAE [2] (Tetrakis dimethylamino ethylene) is probably still the best in terms of quantum efficiency, as is seen in Fig. 1, which compares the TMAE with a CsI solid photocathode. In a wavelength window defined by the transmission of 1 cm of C_6F_{14} liquid, which is frequently used as a Cherenkov radiator, the two quantum efficiencies may differ by almost a factor of two (if one accepts measurements of A. Breskin et.al.[3] as a reference). In addition, TMAE can be delivered in a gaseous form, allowing a continuous replenishing of the photocathode. Furthermore, as observed in the SLD CRID and DELPHI RICH [4], there is no apparent long term loss of efficiency, which may indicate that the long term problems with TMAE handling are under control.

Despite the fact that the TMAE photocathodes were used in a number of large experiments, one still seeks answers to many detailed questions :

(a) How can avalanche photons be quenched ? The avalanche photons may initiate secondary ionization, occurring either in the gas or on TMAE-covered electrode surfaces, thus creating background signals. Many experiments [4] have decided to "baffle" the anode wires using "blind electrodes" to limit the number of such photons either entering the drift volume or striking the neighboring electrode surfaces, where they can cause the secondary photoelectrons. This may help the off-line analysis by simplifying the event, but it doesn't help chamber avalanche quenching issues, and it complicates the mechanical issues for applications involving many short drift cells. Can avalanche photons be intercepted directly at the source, i.e. at the anode wire, by choosing a suitable gas, allowing a simple mechanical structure for the chamber ? We have suggested [5] using the single electron pulse height spectrum as a quantitative measure of quenching. For a sufficiently long charge integrating gate, the secondary pulses will tend to show up as an excess at the large pulse height end of the distribution. When fitting the Polya function, such shape will be parametrized by a negative value of θ. At low gains, typical pulse height spectra are fitted well by an exponential (Furry) distribution; this case corresponds to $\theta=0$. As one increases the gas gain, the Furry distribution typically changes to a Polya distribution with $\theta>0$. However, in a presence of large rate of secondary processes, the exponential distribution turns directly to a distribution with $\theta<0$. These questions can only be answered in the final detector geometry operating with final material choices, gases and voltages. Since this paper is using a test detector, it addresses a gas dependence for a particular cathode material and geometry choice.

(b) Large dE/dx charge deposits in the detector drift volume tend to cause confusion because the electronics is normally tuned for a single electron response. Perhaps there would be an advantage in choosing a helium based gas to minimize dE/dx deposits.

(c) Finally, there is the expected large rate of wire aging in TMAE based gases [6,7].

Our study is related to a development of the Fast Drift CRID [8], which was a candidate for particle identification at the B-factory at SLAC. Fig. 2 shows its basic geometry. It is based on a short drift cell of about 10 cm length, repeated many times. Carbon anode wires of 33 μm diameter are placed 0.8 mm away from the cathode, which consists of metal-plated quartz sheets. The wire-to-wire distance is 5 mm. The coordinate along the length of the cell is measured using drift time, and the coordinate along the width is measured by means of charge division in the resistive carbon wires. The coordinate along the 1.5 cm depth of the cell is obtained from the known wire location. To minimize the radial extent of the detector, we need a short Cherenkov photon conversion length. Therefore, it is necessary to run a high concentration of TMAE, which requires the temperature of the TMAE bubbler to be about 40°C to give a photon absorption length of 6 mm (see CRID and CERES results in Ref. 4). The speed of this detector has to be only as fast as the slowest device in the entire detector system, which is typically the central drift chamber. In our case, the short cell design gives a maximum drift time of 3-4 μsec and a negligible occupancy in the B-factory environment. A description of a prototype device will be described in a subsequent publication. In this paper we concentrate on the gas studies.

The TMAE molecule can be easily photoionized and excited. Its mean ionization potential is only 5.4 eV and its dissociation energy to remove a CH_3 fragment may be as low as 2.7 eV; the molecular structure of TMAE is shown in Fig.3. It is known that there are three excitation carbon lines C*(6.43 eV), C*(7.46 eV), C*(7.94 eV) [1] in the acceptance window defined by the C_6F_{14} transparency and TMAE quantum efficiency (Fig. 1). Such excitations occur during the avalanche and cause the secondary photoelectrons. The excessive production of such hard UV photons can cause not only a background but also chamber instability. To limit the effect of such UV photons, it is necessary to choose a carrier gas which is absorptive to such photons. An obvious candidate is iC_4H_{10}. The low dissociation energy of the TMAE molecule is probably related to a rather high rate of wire aging. One may want to cool the avalanche electrons to reduce their energy below the dissociation energy limit. Again, the best candidate for this is iC_4H_{10}. We have considered three classes of carrier gases : (a) fast gases based on CF_4, to reduce event occupancy, (b) low mass gases based on helium, to minimize the dE/dx tracking deposits in the drift cells, and (c) hydrocarbon based gases (especially iC_4H_{10}-based gases) to obtain adequate quenching. The study of mixtures of such carrier gases with TMAE constitutes the framework of our study.

We are interested in the change of the drift velocity when adding a large amount of TMAE by running the bubbler temperature as high as 40°C; this results in about 0.18% of TMAE relative to the carrier gas. We do not expect the diffusion to be much affected by adding this small amount of TMAE. We are also interested in the single electron pulse height spectra. As mentioned above, if secondary avalanches occur due to insufficient avalanche quenching, the single electron spectra

develop a long tail, providing that the integration time is sufficiently long to accept these secondary processes. We have also performed wire aging studies which will be compared with previously published results [6,7].

It is well known that the CF_4 molecule can absorb an electron and dissociate to form F^- and CF_3^- negative ions as well as F*, CF_2* and CF_3* radicals. The probability for these processes peaks at an electron energy of about 6-7 eV, i.e. the effect occurs only very near the wire when the field is between 8 and 35 kV/cm/atm [9]. An important question is whether these processes will cause a loss of single photoelectrons as they arrive at the avalanche region. The iC_4H_{10} admixture will tend to lower the average electron energy in the avalanche, and therefore it will reduce the probability of the negative ion formation. According to Biaggi's simulation [10], an addition of about 20% of iC_4H_{10} should be sufficient to prevent any losses. However, this has to be yet tested, and is not addressed in this paper.

2. DESCRIPTION OF EXPERIMENTAL APPARATUS.

The drift velocity, single electron pulse height and quenching studies were accomplished using the experimental setup shown in Figure 4. This portion of experiment was performed at SLAC and was described in more detail earlier [5]. A N_2-laser beam was reflected by two mirrors and injected into a drift cell. The position of the second mirror could be controlled using a stepper motor, allowing the laser beam position to be moved in precisely known steps. A portion of the laser beam was reflected to a photodiode which was used to produce a reference start signal for the timing measurements. To ensure that we were dealing with single electrons, the probability of having an event per laser shot was set to less than 10% by attenuating the laser beam.

The drift cell is made of two sections : a drift region made of equally spaced stainless steel rings and a gain region containing a 20 μm gold-plated tungsten anode wire surrounded by a nickel-plated cathode. The gain and the drift regions are separated by a stainless steel foil which has a 330 μm diameter hole, allowing electrons to enter the gain region. The spacers between the stainless steel rings have small openings for the laser beam, allowing a typical step of 5 mm between two laser positions. The drift field was defined by the potentials V_L and V_H . The maximum drift field was typically 2 kV/cm/atm and was limited by either the 10 kV power supply limit or an electrical breakdown originating in the drift structure. The wire gain was controlled by the potentials V_C and V_L. Normally, the gain was kept fixed and the drift field varied by changing the V_H voltage in small steps.

Avalanches initiated by single photoelectrons were detected by an amplifier of the type used for the CRID detectors [4] of the SLD experiment. The amplifier output was split, and using a LRS-612 post-amplifier, the two outputs were discriminated at two different threshold levels. Both signals were then digitized separately in a LRS TDC-2228. The double threshold technique was used to improve the timing resolution of the single electron pulses.

We measured the single electron pulse height spectra using a LRS QVT-3001 operated in the charge integrating mode, with an internal 600 ns gate width. To estimate the wire gain we have calibrated the QVT spectrum by injecting charge into the amplifier input. We fitted the single electron pulse height spectra with a Polya function and estimated the mean "visible" gain from the fit. The visible gain is a portion of the total gain seen by our integration time (600 ns). A correction to get the total wire gain was calculated using a knowledge of the QVT gate width, mobility of positive ions and known time development of the charge, assuming for simplicity a cylindrical geometry. The correction factor was about 1.5-2.0. We also applied a cut on small pulses near the pedestal typically below 2-4 fC, to avoid an unreliable region near the threshold of the internal gating circuit.

For detection of insufficient quenching, we have displayed the amplifier pulses on a digital oscilloscope, HP-54502A, during the measurements. Insufficient quenching would show up either as an irregular shape or as a sequence of multiple pulses following the primary avalanche.

The whole process was controlled by a Macintosh IIcx with a Bergoz MAC-CC controller coupled to CAMAC and GPIB interfaces. The GPIB interface communicated with a Keithley Digital Multi-meter#196 which monitored various analog voltages and resistances. The system recorded gas temperature, barometric pressure, oxygen and water concentration. The software was based on MAC-UA1 software, and included improvements to allow on-line fitting to linear, Gaussian and Polya functions. The measurement operation was completely under computer control, including the laser beam positioning, voltage control of Bertan power supplies, etc. The typical event logging rate was 20 Hz.

The gas mixing was performed using two mass flow controllers [11]. Prior to mixing the flow rate of each controller was calibrated by a soap bubble flow meter. We used an Oxisorb filter [12] and a 13X molecular sieve [13] during all measurements to remove the oxygen and water. However, in case of the CF_4 gas with the TMAE additive, this was not enough : the "99.7% purity" CF_4 gas that we used was normally contaminated by something other than oxygen, but which caused the oxygen cell to read at a level of 30-50 ppm. The oxygen meter used an A2C electrolytic cell [14]. This problem is important for the TMAE work, since a low oxygen level is typically used to "certify" a given gas setup. The oxygen level needs to be below the 1-2 ppm level before tests can continue, because the TMAE molecule is very reactive with oxygen, producing electronegative impurities that affect the electron lifetime. A large production rate of TMAE-oxygen byproducts would also contaminate the gas system. We found that the problem of false oxygen readings can be solved by adding a silica gel [15] and an elemental copper filter [16]. Neither the Oxisorb nor the 13X molecular sieve filters solved this problem. We achieved a 0.3 ppm level of oxygen after the elemental copper filter was introduced, at a flow rate of about 50 cc/min. The silica gel filter is there to protect the active surfaces of the elemental copper, which

actually perform the cleaning. The water level in the carrier is less critical for the tests using TMAE. The 13X molecular sieve filter was used, obtaining about 1-2 ppm of H_2O. It is possible to buy CF_4 of "99.999% purity", but it is very expensive. Without the above mentioned special filtering with the elemental copper, we obtained 2-3 ppm of oxygen, and used that solution in several tests performed at LBL and at the Weizmann institute [17]. However, in the SLAC gas system, we normally used CF_4 of "99.7% purity" with the filtering described above. Table 1 shows the purity and sources of gases used in this paper.

TMAE was added to the carrier gas by bubbling the gas through liquid TMAE. The TMAE bubbler temperature was set between 15°C and 40°C, corresponding to a TMAE vapor pressure between 0.24 and 1.36 Torr. The TMAE vapor pressure as a function of temperature was calculated according to the Clausius-Clapeyron equation :

$$P = A \exp[B(\frac{1}{T_o} - \frac{1}{T})], \qquad (1)$$

where T is temperature in degrees Kelvin, T_o is a reference temperature, and P is the vapor pressure in Torr. Anderson [2] has determined A = 0.500 Torr, B = 6372°K, T_o = 300°K. The Delphi RICH group quoted slightly different values [18] : A = 0.563 Torr, B = 6285°K and T_o = 300°K. We will use the Delphi's values in this paper.

The TMAE used in the present tests was cleaned by the same technique used for the CRID detector [4] by (a) washing it with deionized water, (b) filtering through silica gel, 3A and 5A molecular sieves, and (c) keeping it under partial vacuum by pumping at about 1-3 Torr for 15-20 hours. In the earlier TMAE wire aging tests [6], the vacuum pumping step was not performed.

The detector vessel temperature was set about 10°C higher than the bubbler temperature to prevent condensation. Small variations of temperature during a measurement were corrected to a nominal detector temperature T, i.e., the calculation of E/p is quoted at T+273, where T is the detector temperature in a given measurement. In this paper we quote results at two nominal temperatures, at 298 and 323°K. Similarly, small variations of pressure were corrected to a nominal pressure of 1 atm = 1013.6 mb.

The wire aging studies were performed at LBL using two types of detectors. The first type of detector is shown in Figure 5a and was described in more detail in reference 6 and 7. All tests used a 5 mCi Fe^{55} radiation source. The Fe^{55} X-rays had to penetrate a stainless steel foil of 12 μm thickness before entering the active volume of the chamber. Various types of anode wires were placed into a cathode slot, which had the same geometry as the CRID detectors [4]. The cathode was made of nickel plated aluminum, the plating technique used was the electroless nickel process. A typical initial current was about 100-200 nA at a CRID operating point that corresponds to a total wire gain of about $2x10^5$. The source illuminated about 5 mm of wire length on average. The second type of detector used in the wire aging study had 10 mm inside diameter copper tubes, with

a thin aluminum window to allow the Fe^{55} source X-rays to penetrate into the active volume of the tube (Fig. 5b). The tube used 50 μm gold-plated tungsten anode wire. In this case, the source illuminated about 3 mm of wire length.

3. EXPERIMENTAL RESULTS.

3.1. Quenching properties of TMAE-laden gases.

3.1.1. CF_4+TMAE

The principle motivation to try this particular gas was its high electron drift velocity. There would also be a considerable operational advantage in using a single-component carrier gas.

We immediately noticed that this particular gas mixture has difficulty quenching adequately, resulting in frequent chamber trips. Insufficient quenching is caused by an inability of the avalanche to extinguish itself : the avalanche breeds another one creating an instability. This secondary avalanche breeding is illustrated by the single electron pulses shown in Figure 6. Figure 6a shows a reasonably well behaved single electron pulse in CF_4 gas without TMAE. This is to be compared to Figure 6b showing poorly quenched pulses in CF_4+TMAE gas with TMAE bubbler at 40°C and the detector at 50°C. The pedestal is not shown because there were too many events with no signal, due to the small probability to detect a single photoelectron (causing the QVT overflows). The poor quenching is accompanied by formation of many pulses corresponding to multiple avalanches. Subsequently we found an explanation for this effect [19] : CF_4 has a very strong emission line near 165 nm, which can easily ionize TMAE molecule. This may explain above mentioned "bad quenching behavior" of this gas. The CF_4+TMAE gas is the only gas where we have seen a long tail (10-20 ns) in the distribution of time arrival of the charge. Nominally this distribution is close to Gaussian [5]. The reason for the tail is probably a delay due to deexcitation of CF_4 molecules. Our work motivated enough interest to promote further study on the CF_4 scintillation in reference 17.

The insufficient quenching in CF_4+TMAE gas can be quantified by measuring the single electron pulse height spectra [5]. If the avalanche breeding or the secondary cathode processes cause the chamber pulses to look like those in Figure 6b, single electron pulse heights start developing an excess at the large pulse side of the spectrum, provided that the integration gate is sufficiently long. The Polya distribution parameter θ may be a good parameter for indicating a development of a long tail in the pulse height spectrum, if "avalanche breeding" occurs. The Polya function is defined as follows :

$$P(q) \cong \left[(1+\theta)\frac{q}{\bar{q}}\right]^{\theta} e^{-(1+\theta)(q/\bar{q})}$$

where q is the number of electrons in the avalanche and $\bar{q}$ is the corresponding mean number of electrons. A positive value of θ indicates good quenching, while a negative value θ indicates poor

quenching. Table 2 shows our results for various gases. One can see that CF_4+TMAE gases have very negative values of θ, supporting our model.

However, there is another way to recognize poor quenching. If the single electron pulse height spectrum is plotted on a logarithmic scale, a negative value of θ corresponds to a case when an excess is observed above a linear decrease at large pulse heights, i.e. the decrease is slower than exponential. To illustrate this behavior, Fig. 7 shows a comparison of single electron spectra of CF_4+TMAE and CF_4. Fig. 7a shows the spectrum in a "new chamber" (see below) with the CF_4 gas (detector at 25^{o}C), Fig. 7b shows the same for CF_4+TMAE (bubbler at 15^{o}C; detector at 30^{o}C) and Fig. 7c the same for even higher TMAE concentration (bubbler at 40^{o}C; detector at 50^{o}C).

In addition to two previously mentioned characteristics, one can also observe a very large dependence of the wire gain on the voltage in poorly quenched gases. Among the gases presented in Table 3, the CF_4+TMAE has the largest sensitivity of gain to voltage. Furthermore, the CF_4+TMAE gas has a tendency to create the self-sustaining cathode currents triggered by an intense radioactive source, simulating high background conditions.

Finally, we would like to mention a phenomenon of "photosensitive memory". Once the TMAE was introduced to the chamber operating with CF_4 gas, the chamber had a "memory" of the TMAE even after a very extended period of 5 weeks with N_2 gas flowing (vacuum pumping was not possible in this case). Such a TMAE exposed chamber, operating with the CF_4 gas, never reaches the same maximum wire gain compared to a "new chamber" prior the introduction of TMAE. The exposed chamber behaved as if the cathode surfaces were photo-sensitized and that the avalanche photons from the CF_4 excitation drove the chamber easily into an instability (we think that there remains some residual contamination of TMAE or its reaction products on the surfaces, causing this behavior).

3.1.2. CF_4+iC_4H_{10}+TMAE.

Adding 20% or more of iC_4H_{10} to CF_4+TMAE greatly improves the chamber quenching behavior. For example, it could again reach its pre-TMAE "new chamber" operating voltages without any problem. Fig. 8 shows single electron spectra in CF_4+iC_4H_{10}+TMAE gases. Fig. 8a shows 80%CF_4 +20%iC_4H_{10} (no TMAE; detector at 25^{o}C) gas with a positive θ = +0.324 (see Table 2), indicating sufficient quenching. However, Fig. 8b indicates that addition of TMAE (bubbler at 40^{o}C; detector at 50^{o}C) makes θ negative (θ = -0.636). More iC_4H_{10} is needed to stabilize the avalanche process. Fig. 8c indicates that 32% of iC_4H_{10} gives just about exponential behavior (θ~0). Fig. 8d indicates further improvement in quenching as more iC_4H_{10} is added; in this case the mixture is 63.5% CF_4 +36.5% iC_4H_{10} (bubbler at 40^{o}C; detector at 50^{o}C) yields θ= +0.626. This result suggests that θ is very sensitive.

Fig. 9 shows voltage-gain characteristics for two groups of gases, one is CF_4+TMAE, and the other is a better quenched CF_4+ iC_4H_{10}+TMAE. One can see that CF_4, if mixed with TMAE, has much steeper gain dependency on the voltage compared to CF_4+iC_4H_{10}+TMAE. Table 3 shows this quantitatively. It indicates that the slope dG/dV is a sensitive indicator of poor quenching : CF_4+TMAE gas (TMAE bubbler at 40^{o}C and the detector at 50^{o}C) has the worst quenching of all gases we have tested, and has also the largest slope.

3.1.3. CH_4+TMAE.

Fig. 10a shows the CH_4 pulse height spectrum without the TMAE. Fig. 10b indicates that CH_4+TMAE has quenching difficulties somewhat similar to those of CF_4+TMAE, although to much lesser extent. Confirmation of this is given in Table 2, where θ is seen to change from +0.422 to -0.093 as the gas is changed from CH_4 to CH_4+TMAE.

3.1.4. C_2H_6+TMAE.

This particular gas is used in the SLD Barrel CRID [4]. There is direct experience with the rate of secondary avalanche hits in the SLD experiment, which gives us a chance to "calibrate" our quenching model. The observed rate of secondary photoelectrons in the drift volume is about 1% for every primary single electron avalanche. By removing the photon blocking electrode structure (blinds) in the SLD Barrel CRID [4], one would keep a simple wire geometry as is planned for the Fast Drift CRID (Fig. 2), and the rate of secondary photoelectrons would increase to 7-8%. Our test, as one can see in Fig. 11 and Table 2 indicates that C_2H_6+TMAE belongs to the category of well-quenched gases (θ=+0.235), according to our model.

3.1.5. iC_4H_{10}+TMAE.

Fig. 12 and Table 2 clearly indicate that iC_4H_{10}+TMAE is one of the best quenched gases we have tested (θ=+0.639). In addition, the gain-voltage dependence is smallest (Fig. 13 and Table 3).

3.1.6. CO_2+C_2H_6+TMAE.

This gas is used in the SLD Endcap CRID [4], which needs a slower gas to reduce the Lorentz angle due to the ExB effect. Fig. 14 show the pulse height spectra. A comparison of Fig. 14b with Fig. 11b shows that this gas has somewhat poorer quenching behavior than the SLD Barrel CRID gas C_2H_6+TMAE. Table 2 indicates θ=+0.107 for 15%CO_2+ 85%C_2H_6+TMAE gas compared to θ=+0.235 for C_2H_6+TMAE. Table 3 indicates that the CO_2/C_2H_6/TMAE also has a steeper gain-voltage dependence. Although there is this difference between these two gases using our quenching model, the SLD Endcap CRID operates successfully. However, based on tests at SLD, only ~100 extra Volts is needed on the cathode to drive a very large fraction of events into pulse height saturation, indicating that the gas may be sensitive to the quenching problem.

3.1.7. He+iC_4H_{10}+TMAE.

Fig. 15 shows several single electron pulse height spectra from tests of He+iC_4H_{10}+TMAE mixtures. From Table 2 we can see that about 20% of admixture of iC_4H_{10} in helium appears to provide good quenching (θ=+0.216). However, judging from the gain-voltage dependence (see Table 3), a 40% admixture of iC_4H_{10} is preferable.

3.1.8. He+C_2H_6+TMAE.

From Fig. 16 and Table 2 we conclude that 50%He+50%C_2H_6+TMAE has sufficient quenching (θ=+0.273).

3.2. Drift velocity.

It is important to understand the effect on the drift velocity of adding a relatively large amount of TMAE. In the case of very fast CF_4 based mixtures, the effect of TMAE is to reduce the drift velocity, while in the case of the helium-based gases, the effect is to increase the drift velocity.

Fig. 17 shows a comparison of the drift velocity for CF_4 (no TMAE, detector at 25^{o}C), CF_4 + TMAE (bubbler at 15^{o}C, detector at 30^{o}C), and CF_4 + TMAE (bubbler at 40^{o}C, detector at 50^{o}C). One can see that a relatively large addition of TMAE (~0.18% relative to the carrier gas) lowers the drift velocity only at the lower fields, and the gas still remains fast.

Fig. 18 shows a comparison of the drift velocity between 80%CF_4 +20%iC_4H_{10} (no TMAE, detector at 50^{o}C), 80% CF_4 +20% iC_4H_{10} + TMAE (bubbler at 40^{o}C; detector at 50^{o}C), 68% CF_4 +32% iC_4H_{10} + TMAE (bubbler at 40^{o}C; detector at 50^{o}C), and 63.5% CF_4+36.5% iC_4H_{10}+TMAE (bubbler at 40^{o}C; detector at 50^{o}C). It is apparent that this group of gases containing iC_4H_{10} is already somewhat slower than the CF_4 gas.

Fig. 19 shows the drift velocity in slower gases C_2H_6, iC_4H_{10}, 50% He+50% C_2H_6 , 15% CO_2+85% C_2H_6, 80% He+20% iC_4H_{10}, 60% He+40% iC_4H_{10} with and without TMAE addition (bubbler at 40^{o}C; detector at 50^{o}C).

One can conclude that if one chooses iC_4H_{10}+TMAE gas because of the quenching argument, the Fast Drift CRID will achieve ~3.3 $cm/\mu sec$ at 1 kV/cm; a choice of 60% He+40% iC_4H_{10} gives ~2.9 $cm/\mu sec$. Therefore, in the Fast Drift CRID design, the ten cm drift will require up to ~3 μsec.

3.3. Wire aging.

One does expect a high rate of polymerization in TMAE-laden gases because the low mean ionization potential of the TMAE molecule, 5.4 eV, provides the photoionization capability, and because the N-CH_3 bond strength is less than 3 eV, giving a high degree of fragility (see Fig.3).

Early tests were performed at SLAC in the apparatus described by Fig. 5a [6]. Recently, some of the tests were repeated in the same apparatus including different wire diameters and gases. The tests included not only the anode wire aging, but also measurement of charging effects and self-sustaining cathode currents [7]. To verify and complement the SLAC wire aging results in a

completely different setup, we also performed the wire aging tests at LBL in a setup described earlier [20].

It is useful to remind the reader of the non-TMAE results first [21]. It was observed earlier that the pure CF_4 has a very rapid aging rate. The wire gain drops by more than 100000 %/C/cm in the first few mC of a charge dose. This was not expected since we did measure very low aging rates with mixtures such as $80\%CF_4+20\%iC_4H_{10}$. A model explaining this effect is given in references 20 and 21 and indicates that the problem is caused by the cathode related effects .

Fig. 20 shows two wire aging results with CF_4+TMAE; with the TMAE bubbler operating at 40.6ºC and the detector at 50ºC : (a) with 33 μm diameter carbon wire in the detector of Fig. 5a and (b) with 50 μm diameter gold plated tungsten wire in the detector of Fig. 5b. In both types of detectors we have observed a seemingly strange result . The current would initially drop, as in a normal wire aging experiment, but after few minutes the current would slowly start increasing, as if the cathode were coated with some photosensitive material which produced a photocurrent initiated by the photons from the avalanche. At that time we did not yet know that the CF_4 is a very good emitter of photons in a form of scintillation light at about 165 nm, just at a wavelength where TMAE has large quantum efficiency [17,19]. As the cathode deposits build up during the wire aging test, a photocurrent triggered by the CF_4 excitations increases, causing the behavior seen in Fig. 20. In addition, it was also noted that the chamber would rather easily develop self-sustaining cathode currents, i.e. currents which would persist even when the source was removed.

The gas $80\%CF_4+20\%iC_4H_{10}$+TMAE exhibits the usual wire aging behavior for TMAE, i.e. a rather smooth decrease as a function of charge dose. Fig. 21 shows experimental results with this gas together with the previous results [6,7]. It is seen that the use of larger diameter anode wire reduces the wire aging rate. For large anode wires the TMAE aging rate is comparable to the aging rate of a chamber without the TMAE. This confirms the old result which showed that the larger the anode wire diameter, the smaller the wire aging rate [6,7]. Fig. 22 shows that the wire aging rate is independent of TMAE concentration. This also confirms the previous results [6,7].

We also have confirmed the previous results [6,7] that the wire aging deposits can be evaporated by passing a small current through the wire and heating it. In Fig. 22 we used one "new" and two "regenerated" wires. In this particular case we used the 33 μm diameter carbon wire, ~70 Volts across the wire and ~40 mA current for about 2 minutes.

For a comparison, we have also performed some non-TMAE wire aging tests to see how they differ from those for the TMAE-laden helium mixtures. Table 4 summarizes all results including the previous results given in reference 6 and 7. Notice that the helium based non-TMAE results are about 1000 times better than the results with TMAE.

4. CONCLUSIONS

a) We have investigated criteria for quenching in avalanche counters using a quantitative model

[5] based upon the Polya function fits to the single electron pulse height spectrum. This model has been successfully applied to gases with and without TMAE. From the fitted mean charge $\overline{q}$, we have determined the wire gain, and from the parameter θ, we can predict the quenching capability. A positive value of θ indicates good quenching, while a negative θ indicates poor quenching. According to this model one should choose a gas with the largest possible positive θ.

b) Increased TMAE concentration causes a decrease in θ.

c) The CF_4 +TMAE mixture is the poorest gas we have tested with regard to quenching. We believe this is because photons from avalanche-excited CF_4 molecules are in the TMAE photoionization window. This gas is also very prone to excitation of self-sustaining currents. We think that this gas would be a very bad choice.

d) We recommend adding at least 50% of iC_4H_{10} to the CF_4 +TMAE mixture to ensure good quenching.

e) CH_4+TMAE exhibits quenching difficulties similar to those of CF_4+TMAE, but to a much smaller degree.

f) The best quenching candidate for the Fast CRID is iC_4H_{10}+TMAE.

g) He+TMAE with admixture of 20-40% of iC_4H_{10} is also an interesting choice, because it would reduce dE/dx deposits in the chamber.

h) A relatively large addition of TMAE (40^{o}C bubbler temperature), does not alter the drift velocity significantly. In CF_4-based gases, the drift velocity is decreased, while in the helium-based gases the drift velocity is increased.

i) We have confirmed the previous wire aging results [6,7], that the TMAE wire aging deposits can be removed by heating the carbon anode wire with a small current, and that the rate of aging is inversely proportional to the anode wire diameter.

ACKNOWLEDGEMENTS

We thank M. McCulloch for excellent technical support during this test.

FIGURE CAPTIONS

1. Quantum efficiency of TMAE compared to CsI [3]. The graph also shows a transmission of 1 cm of C_6F_{14} liquid, which is a typical radiator in the CRID detectors, and defines a short wavelength acceptance edge.
2. Fast CRID with short drift cell geometry and no blind structure blocking the avalanche photons.
3. TMAE (Tetrakis dimethylamino ethylene) molecular structure.
4. Experimental setup used to measure the drift velocity, single electron pulse height spectra and quenching characteristics.

5. (a) The first setup used to perform the wire aging and rate dependent effects at SLAC in references 6 and 7; (b) The second setup to perform the wire aging at LBL.
6. Examples of (a) well quenched single electron pulse in CF_4 gas, and (b) poorly quenched pulses using CF_4+TMAE gas (bubbler at 40^{o}C; the detector at 50^{o}C), which demonstrate avalanche breeding.
7. Our measurements of single electron spectra (a) in the "new chamber" with the CF_4 gas (detector at 25^{o}C); (b) for CF_4+TMAE (bubbler at 15^{o}C; detector at 30^{o}C); (c) for CF_4+ TMAE (bubbler at 40^{o}C; detector at 50^{o}C). Solid line is an indication of exponential shape.
8. Our measurements of single electron spectra in (a) 80% CF_4+20% iC_4H_{10} (no TMAE; detector at 25^{o}C), $\theta > 0$; (b) 80% CF_4+20% iC_4H_{10} +TMAE (bubbler at 40^{o}C; detector at 50^{o}C), $\theta < 0$; (c) 68% CF_4 +32% iC_4H_{10} +TMAE (bubbler at 40^{o}C; detector at 50^{o}C), $\theta \sim 0$; (d) 63.5% CF_4 +36.5% iC_4H_{10}+TMAE (bubbler at 40^{o}C; detector at 50^{o}C), $\theta > 0$. Solid line is an indication of exponential shape.
9. Our measurements of voltage-gain characteristics for CF_4+TMAE (bubbler at 15^{o}C; detector at 30^{o}C; closed squares), CF_4+TMAE (bubbler at 40^{o}C; detector at 50^{o}C; closed circles), 80%CF_4 + 20%iC_4H_{10}+TMAE (bubbler at 40^{o}C; detector at 50^{o}C; open squares), 68%CF_4+ 32%iC_4H_{10}+TMAE (bubbler at 40^{o}C; detector at 50^{o}C; open diamonds), 63.5%CF_4+36.5%iC_4H_{10}+TMAE (bubbler at 40^{o}C; detector at 50^{o}C; + points), 80%CF_4+ 20%iC_4H_{10} (no TMAE; detector at 25^{o}C; open circles).
10. Our measurements of single electron spectra in (a) the CH_4 gas (detector at 25^{o}C); (b) for CH_4+TMAE (bubbler at 40^{o}C; detector at 50^{o}C). Solid line is an indication of exponential shape.
11. Our measurements of single electron spectra in (a) the C_2H_6 gas (detector at 25^{o}C); (b) for C_2H_6+TMAE (bubbler at 40^{o}C; detector at 50^{o}C). Solid line is an indication of exponential shape.
12. Our measurements of single electron spectra in (a) the iC_4H_{10} gas (detector at 25^{o}C); (b) for iC_4H_{10}+TMAE (bubbler at 40^{o}C; detector at 50^{o}C). Solid line is an indication of exponential shape.
13. Our measurements of voltage-gain characteristics for (a) non-TMAE gases (detector at 50^{o}C) :

    80%He+ 20%iC_4H_{10} (open circles), 50%He+ 50%C_2H_6 (open diamonds), C_2H_6 (closed squares), 15%CO_2+85%C_2H_6 (+ points), iC_4H_{10} (closed circles), (b) TMAE laden gases (bubbler at 40^{o}C; detector at 50^{o}C) : 80%He+ 20%iC_4H_{10}+TMAE (open circles), 50%He+ 50%C_2H_6+TMAE (open diamonds), 60%He+ 40%iC_4H_{10}+TMAE (closed diamonds), 15%CO_2+85%C_2H_6+TMAE (+ points), C_2H_6+ TMAE(closed squares), CH_4+ TMAE (open squares), iC_4H_{10}+ TMAE(closed circles).

14. Our measurements of single electron spectra in (a) the 15%CO_2+85%C_2H_6 gas (detector at 25^{o}C); (b) for 15%CO_2+85%C_2H_6+TMAE (bubbler at 40^{o}C; detector at 50^{o}C). Solid line is an indication of exponential shape.
15. Our measurements of single electron spectra in (a) 80% He+20%iC_4H_{10} (no TMAE; detector at 25^{o}C), $\theta > 0$; (b) 80% He+20% iC_4H_{10} +TMAE (bubbler at 40^{o}C; detector at 50^{o}C), $\theta \sim 0$; (c) 60% He +40%iC_4H_{10} +TMAE (bubbler at 40^{o}C; detector at 50^{o}C), $\theta > 0$. Solid line is an indication of exponential shape.
16. Our measurements of single electron spectra in (a) the 50%He+50%C_2H_6 gas (detector at 25^{o}C); (b) for 50%He+50%C_2H_6+TMAE (bubbler at 40^{o}C; detector at 50^{o}C). Solid line is an indication of exponential shape.
17. Our measurement of the drift velocity for CF_4 (no TMAE; detector at 25^{o}C; closed circles), CF_4+TMAE (bubbler at 15^{o}C; detector at 30^{o}C; open squares), and CF_4+TMAE (bubbler at 40^{o}C; detector at 50^{o}C; open circles). Curve is only for eye guidance.
18. Our measurement of the drift velocity for 80% CF_4 +20% iC_4H_{10} (no TMAE; detector at 50^{o}C; closed circles), 80% CF_4 +20% iC_4H_{10} + TMAE (bubbler at 40^{o}C; detector at 50^{o}C; open squares), 68% CF_4 +32%iC_4H_{10}+TMAE (bubbler at 40^{o}C; detector at 50^{o}C; open circles), and 63.5% CF_4 +36.5% iC_4H_{10}+TMAE (bubbler at 40^{o}C; detector at 50^{o}C; closed squares). Curves are only for eye guidance.
19. Drift velocity in various gases : (a) with no TMAE and 24^{o}C detector temperature : C_2H_6 (open squares), iC_4H_{10} (closed squares), 50% He+50% C_2H_6 (open circles), 15% CO_2+85% C_2H_6 (open diamonds), 80% He+20% iC_4H_{10} (closed circles); (b) with 40^{o}C TMAE bubbler and 50^{o}C detector temperature : C_2H_6 (open squares), iC_4H_{10} (closed squares), 50% He+50% C_2H_6 (open circles), 15% CO_2+85% C_2H_6(open diamonds), 80% He+20% iC_4H_{10} (closed circles); 60% He+40% iC_4H_{10} (crosses). Curves are only for eye guidance.
20. New wire aging results with CF_4+TMAE, with the TMAE (40^{o}C bubbler; 50^{o}C detector; open squares) in the detector of Fig. 5a with a 33 μm diameter carbon wire; the same, but in the detector of Fig. 5b with 50 μm diameter gold plated tungsten wire (open circles).
21. New wire aging results in 80%CF_4+20%iC_4H_{10} gas (no TMAE; detector at 24^{o}C; open triangles) in the detector of Fig. 5b with a 50 μm diameter gold plated tungsten wire; the same, but with TMAE (15^{o}C bubbler; open circles); in 80%CF_4+ 20%iC_4H_{10} gas with TMAE (40^{o}C bubbler; detector at 47.6^{o}C; open squares) in the detector of Fig. 5a with a 33 μm diameter carbon wire; in C_2H_6 with TMAE (27^{o}C bubbler; detector at 40^{o}C; open diamonds) in the detector of Fig. 5a with 7 μm diameter carbon wire (CRID Barrel condition).

22. New wire aging results in 80%CF_4+20%iC_4H_{10} gas with TMAE (40.6ºC bubbler; detector at 47.6ºC; open circles) in the detector of Fig. 5a with a "regenerated" 33 μm diameter carbon wire; the same with the detector at 61.5ºC (open diamonds); the same with a "new" wire, detector at 24ºC and TMAE bubbler at 17.8ºC (open squares).

REFERENCES

[1] J. Sequinot and T. Ypsilantis, Nucl.Instr.&Meth., A343(1994)1 and A343(1994)30.

[2] D. Anderson, Nucl.Instr.&Meth., A270(1988)416, and IEEE Trans.Nucl,Sci, NS-28(1981)842.

[3] A. Breskin, R. Chechik, D. Vartsky, G. Malamud and P. Mine', Nucl.Instr.&Meth. A343 (1994) 159,
J. Sequinot, G. Charpak, Y. Giomataris, V. Peskov, J. Tischauser and T. Ypsilantis, Nucl.Instr.&Meth. A314 (1992) 465,
R.A. Holroyd, J.M.Preses, C.L. Woody and R.A. Johnson, Nucl.Instr.&Meth. A261 (1987) 440,
D.F. Anderson, S. Kwan, V. Peskov and B. Hoeneisen, Nucl.Instr. &Meth. A323 (1992) 626,
C.Lu and K.T.McDonald, Nucl.Instr.&Meth., A343(1994)135.

[4] SLD CRID : A. Abe et. al., Nucl.Instr.&Meth., A343 (1994) 74.
DELPHI RICH : W. Adam et. al., Nucl.Instr.&Meth., A343 (1994) 68.
OMEGA RICH : H.W. Siebert et. al., Nucl.Instr.&Meth., A343 (1994) 60.
CERES : R. Baur et. al., Nucl.Instr.&Meth., A343 (1994) 87.

[5] J. Va'vra, P. Coyle, J. Kadyk and J. Wise, Nucl.Instr.&Meth., A324(1993)113.

[6] J. Va'vra, IEEE Trans. Nucl. Sci., NS 34, No.1, p.486, February 1987; CRID Note #36, SLAC, 1987 and Nucl. Sci., NS 35, No.1, p.487, February 1988.

[7] J. Va'vra, SLAC-PUB-95-6759 and submitted to Nucl.Instr.&Methods.

[8] J. Va'vra, B-Factory note #87, S.L.A.C., November 9, 1992

[9] P. G. Datskos, J.G. Carter and L.G. Christophorou, J.Appl.Phys., 71(1992)15.

[10] S. Biaggi, private communication.

[11] Datametrix Model 825, Edwards High Vacuum, Grand Island, NY14072, U.S.A.

[12] Oxisorb made by Messer Griesheim GmbH, 4000 Dusseldorf, Germany.

[13] 13X Molecular Sieve made by Union Carbide Co., Danburg, CT 06817-0001, U.S.A.

[14] Teledyne Analytical Instr., City of Industry, CA 91748, U.S.A.

[15] Silica Gel Sorbead R was purchased from Adcoa Co., Gardena, CA 90247, U.S.A.

[16] Elemental Copper is made by Engelhard Co., Elyria, OH 44035, U.S.A.

[17] A. Pansky, A. Breskin, A. Buzulutskov, R. Chechik, V. Elkind and J. Va'vra,

WIS-94/23/May-PH and Nucl.Instr.&Meth. A354 (1995) 262.
[18] Y. Giomataris, J.M. Presses, S. Maltezoz, and E. Rosso, DELPHI 86-17 (1986).
[19] J. Friese, R. Gernheauser, G. Montermann and K. Zeitelhack, Physik-Department E12, TU-Munchen, Germany, unpublished report.
[20] J. Wise, "Chemistry of Radiation Damage to Wire Chambers", Ph.D. thesis, LBL-32500, August 1992, and IEEE Trans.Nucl.Sci. NS-37 (1990) 478.
[21] J. Wise, J. Kadyk and D.W. Hess, J. Appl. Phys. 74 (9), p.5327, November 1993.

Table 1 - Purity of gases used in this work

Gas	*Source of gas*	*Specification of purity*	*Used in graph # or Table #*
C_2H_6	*Liquid Belge*	*Very high purity; used in the SLD CRID*	*11,12,14,16,19*
C_2H_6	*Matheson*	*"CP - Grade"*	*21*
He	*Matheson*	*99.999 %*	*11,15,16,19,21,*
CO_2	*Liquid Carbonics*	*99.998 %*	*14, 19*
iC_4H_{10}	*Matheson*	*99.5 %*	*8, 9 , 13, 15, 18, 19 , 21, 22*
CF_4	*AlphaGaz*	*99.999 %*	*20, 21, 22*
CF_4	*Liquid Carbonics*	*99.7 %*	*6,7 ,8, 9, 17, 18, 19*
CH_4	*Matheson*	*"CP - Grade"*	*10*

Table 2 - Summary of Polya fits to single electron pulse heights

(20 μm wire diameter, E_a is electric gradient on the anode wire surface, V_C is cathode voltage, θ is a Polya function parameter and n_D is number of degrees of freedom).

Gas	Vc [kV]	Approx. Ea [kV/cm]	Mean visible charge $\bar{q}$ [e^-]	θ	χ^2 / n_D
CF_4 *(wire at 24°C)*	-1.95	~396	7.5×10^5	+0.209 ±0.024	1.02
CF_4+TMAE *(bubbler at 15°C, wire at 24°C)*	-1.62	~334	2.3×10^5	-0.553 ±0.008	1.22
CF_4+TMAE *(bubbler at 40°C, wire at 50°C)*	-1.415	~295	1.7×10^5	< -0.999	>10
80%CF_4+20%iC_4H_{10} *(wire at 24°C)*	-1.75	~358	3.2×10^5	+0.324 ±0.037	1.39
80%CF_4+20%iC_4H_{10}+TMAE *(bubbler at 40°C, wire at 50°C)*	-1.605	~331	1.3×10^5	-0.636 ±0.004	1.98
68%CF_4+32%iC_4H_{10}+TMAE *(bubbler at 40°C, wire at 50°C)*	-1.606	~331	1.6×10^5	+0.014 ±0.018	1.61
63.5%CF_4+36.5%iC_4H_{10}+TMAE *(bubbler at 40°C, wire at 50°C)*	-1.605	~331	1.6×10^5	+0.626 ±0.015	2.74
CH_4 *(wire at 24°C)*	-1.806	~369	3.0×10^5	+0.422 ±0.010	1.09
CH_4+TMAE *(bubbler at 40°C, wire at 50°C)*	-1.758	~360	2.4×10^5	-0.093 ±0.010	1.29
C_2H_6 *(wire at 24°C)*	-1.806	~369	4.0×10^5	+0.415 ±0.009	0.99
C_2H_6+TMAE *(bubbler at 40°C, wire at 50°C)*	-1.657	~341	2.5×10^5	+0.235 ±0.011	1.16
iC_4H_{10} *(wire at 24°C)*	-1.956	~398	1.8×10^5	+0.733 ±0.008	1.75
iC_4H_{10}+TMAE *(bubbler at 40°C, wire at 50°C)*	-1.956	~398	1.9×10^5	+0.639 ±0.008	1.26
15%CO_2+85%C_2H_6 *(wire at 24°C)*	-1.805	~369	2.9×10^5	+0.409 ±0.021	1.17

15%CO_2+85% C_2H_6+TMAE (bubbler at 40°C, wire at 50°C)	-1.636	~337	1.8×10^5	+0.107 ±0.010	1.16
50%He+50%C_2H_6 (wire at 24°C)	-1.406	~293	2.1×10^5	+0.274 ±0.015	0.90
50%He+50%C_2H_6+TMAE (bubbler at 40°C, wire at 50°C)	-1.274	~268	1.7×10^5	+0.273 ±0.008	1.05
80%He+20%iC_4H_{10} (wire at 24°C)	-1.255	~265	2.8×10^5	+0.338 ±0.021	1.03
80%He+20%iC_4H_{10}+TMAE (bubbler at 40°C, wire at 50°C)	-1.174	~249	1.9×10^5	+0.216 ±0.007	1.04
60%He+40%iC_4H_{10}+TMAE (bubbler at 40°C, wire at 50°C)	-1.374	~287	2.2×10^5	+0.226 ±0.005	1.18

Table 3 - Gain dependence on voltage (20 μm tungsten wire diameter).

Gas	$G(V+100)/G(V)$ at $G_{vis} \sim 2 \times 10^5$ [Gain increase per 100 V]
CF_4 (wire at 24°C)	-
CF_4+TMAE (bubbler at 15°C, wire at 24°C)	7.54
CF_4+TMAE (bubbler at 40°C, wire at 50°C)	11.7
80% CF_4+20% iC_4H_{10}	2.38
80% CF_4+20% iC_4H_{10}+TMAE (bubbler at 40°C, wire at 50°C)	3.95
68% CF_4+32% iC_4H_{10}+TMAE (bubbler at 40°C, wire at 50°C)	3.15
63.5% CF_4+36.5% iC_4H_{10}+TMAE (bubbler at 40°C, wire at 50°C)	2.93
CH_4 (wire at 24°C)	3.06
CH_4+TMAE (bubbler at 40°C, wire at 50°C)	2.80
C_2H_6 (wire at 24°C)	2.34
C_2H_6 +TMAE (bubbler at 40°C, wire at 50°C)	2.34
iC_4H_{10} (wire at 24°C)	2.03
iC_4H_{10}+TMAE (bubbler at 40°C, wire at 50°C)	2.14
15% CO_2+85% C_2H_6 (wire at 24°C)	2.18
15% CO_2+85% C_2H_6+TMAE (bubbler at 40°C, wire at 50°C)	2.76
50% He+50% C_2H_6 (wire at 24°C)	2.84
50% He+50% C_2H_6+TMAE (bubbler at 40°C, wire at 50°C)	2.97
80% He+20% iC_4H_{10} (wire at 24°C)	4.30
80% He+20% iC_4H_{10}+TMAE (bubbler at 40°C, wire at 50°C)	3.31
60% He+40% iC_4H_{10}+TMAE (bubbler at 40°C, wire at 50°C)	2.87

Table 4 - Gain decrease as a function of a charge dose [%/C/cm or %/mC/cm] caused by the anode wire aging; TMAE tests used 33 μm carbon wire diameter (unless specified differently); non -TMAE tests used 20 μm tungsten wire diameter; use a Fe^{55} source to cause the wire damage.

TMAE based gases TMAE : bubbler at 40°C, wire at 50°C	**Gain change as a function of charge dose taken near ~1 mC/cm**	**Total Gain drop after an accumulated charge dose of 1 mC/cm**
	[%/mC/cm]	**[%]**
80% CF_4+20% iC_4H_{10}+TMAE	27.7 ±0.7	~44
80% CF_4+20% iC_4H_{10}+TMAE (50 μm)	11.1 ±2.5	~12
CH_4+TMAE	6.3 ±1.0	~30
C_2H_6 +TMAE	6.2 ±0.6	~15
C_2H_6 +TMAE (7 μm)	14.1 ±0.8	~83
iC_4H_{10}+TMAE	10.2 ±0.5	~28
15% CO_2+85% C_2H_6+TMAE	23.0 ±2.3	~65
50% He+50% C_2H_6+TMAE	15.9 ±1.5	~32
80% He+20% iC_4H_{10}+TMAE	5.8±0.1	~11
60% He+40% iC_4H_{10}+TMAE	13.0 ±0.7	~23

Non -TMAE based gases	**Gain change as a function of charge dose taken near ~80 mC/cm**
	[%/C/cm]
95%He+5%C_2H_6	0.1 ± 0.1
78%He+15%CO_2+7%iC_4H_{10}	30 ±0.2
80% CF_4+20% iC_4H_{10}	4.6 ± 0.1
50% He+50% C_2H_6	23 ± 0.2
70% He+30% C_3H_8	4.4 ± 1.2

Fig.1 7618A20
Fig.2 7872A6
Fig.3 5563A9
Fig.4 6936A1
Fig.5 7618A2
Fig.6 7618A4
Fig.7 7618A11
Fig.8 7618A12
Fig.9 7618A6
Fig.10 7618A22
Fig.11 7618A23
Fig.12 7618A24
Fig.13 7618A15
Fig.14 7618A18
Fig.15 7618A17
Fig.16 7618A16
Fig.17 7618A3
Fig.18 7618A5
Fig.19 7618A14
Fig.20 7618A8

Fig.21 7618A9
Fig.22 7618A10

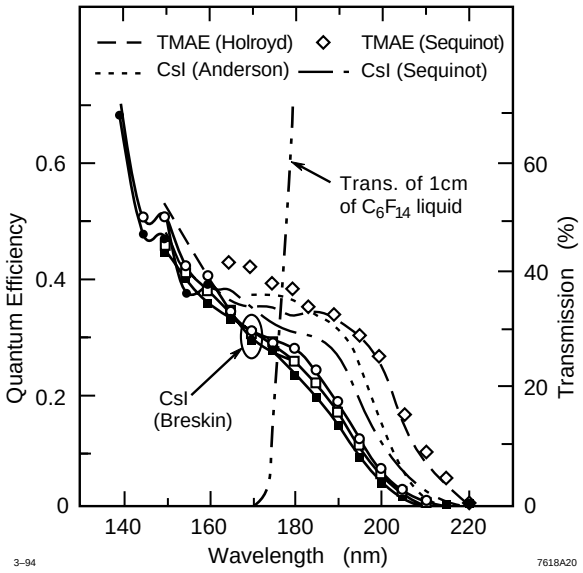

Fig. 1

Figure 1

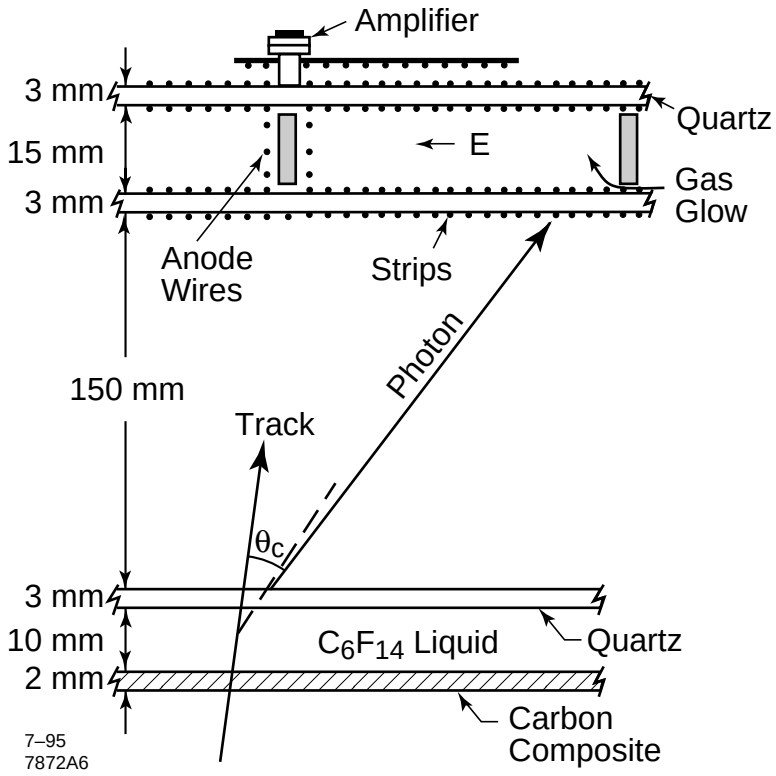
Amplifier
3 mm
15 mm
3 mm
Quartz
E
Gas
Glow
Anode
Wires
Strips
Photon
150 mm
Track
θc
3 mm
10 mm
2 mm
C6F14 Liquid
Quartz
Carbon
Composite
7–95
7872A6

Figure 1:

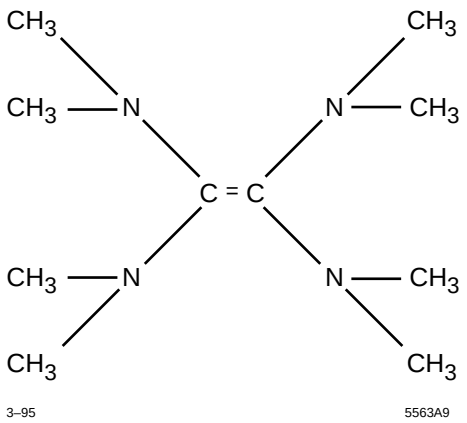

Fig. 3

Figure 2:

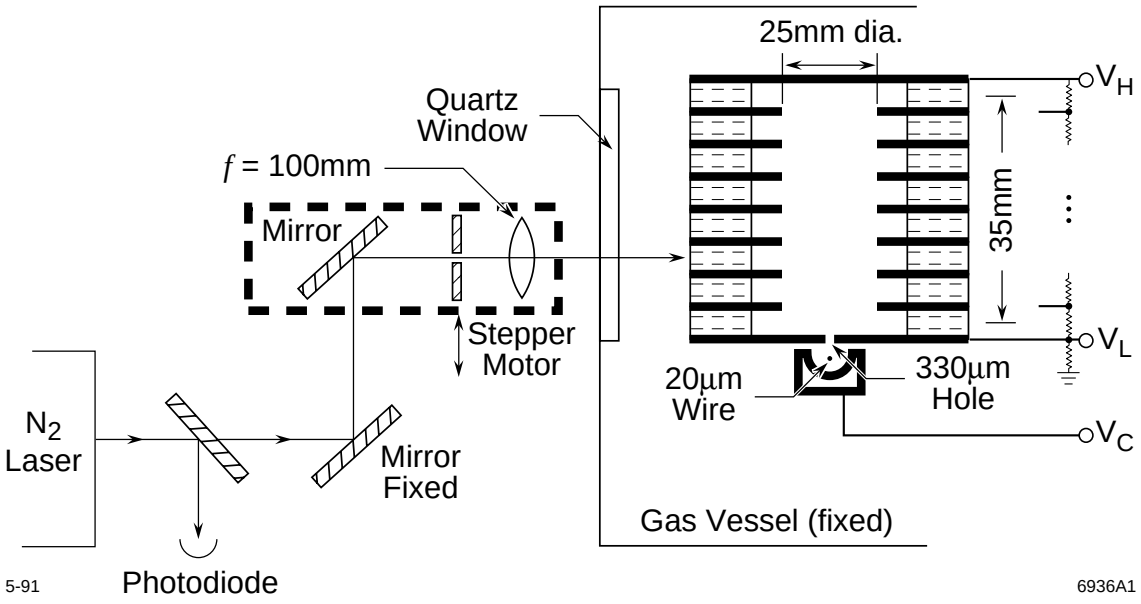
25mm dia.
Quartz
Window
f = 100mm
Mirror
Stepper
Motor
35mm
V_H
V_L
V_C
20μm
Wire
330μm
Hole
N2
Laser
Mirror
Fixed
Photodiode
Gas Vessel (fixed)
5-91
6936A1

Figure 3:

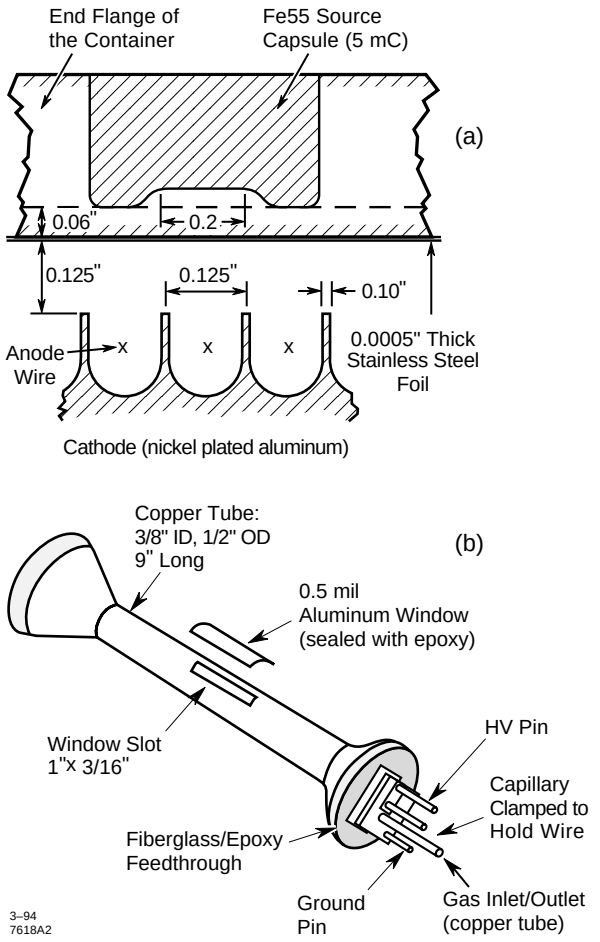

Fig. 1

Figure 4:

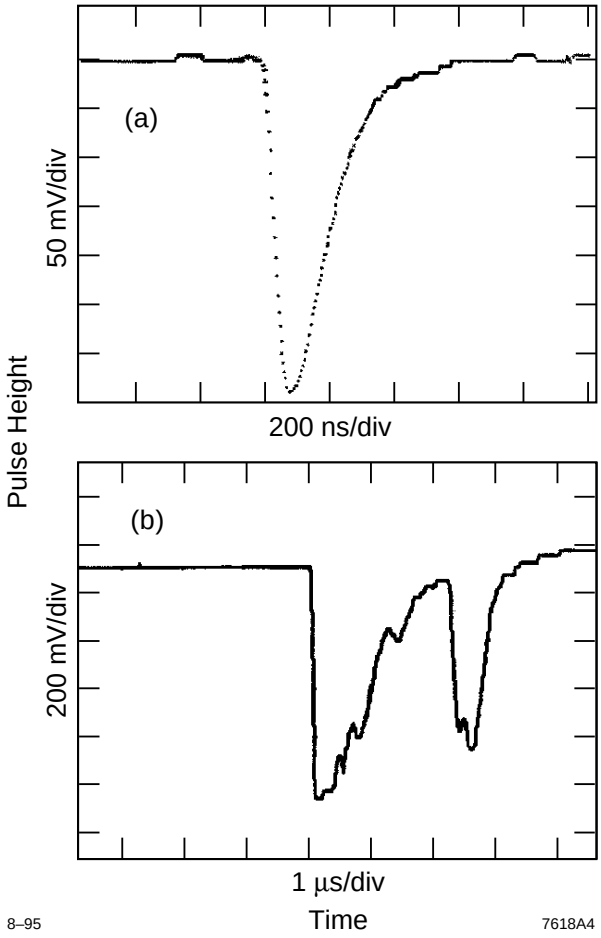

Fig. 3

Figure 5:

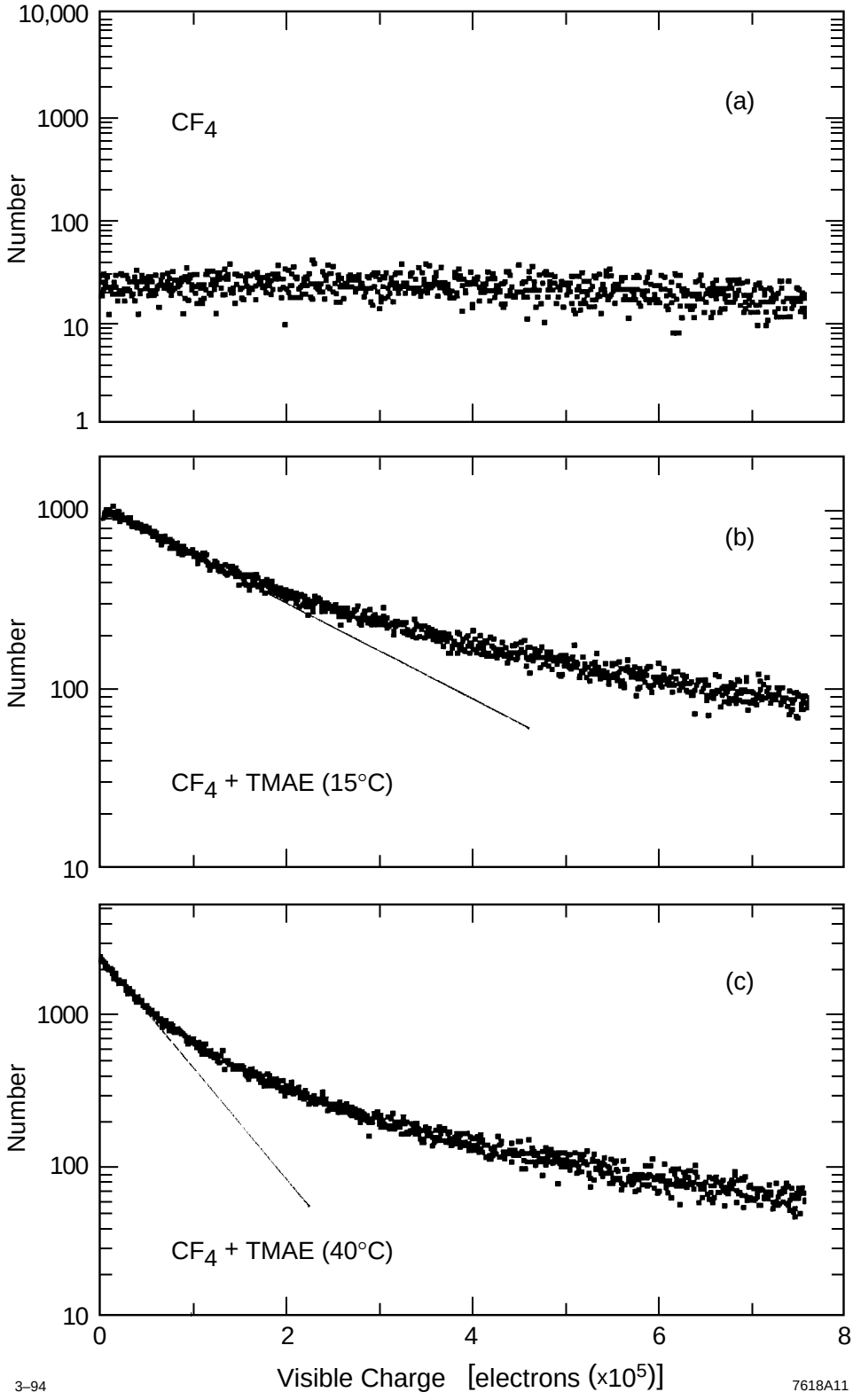
10,000
1000
100
10
1
Number
(a)
CF_4
1000
100
10
Number
(b)
CF_4 + TMAE (15°C)
1000
100
10
Number
(c)
CF_4 + TMAE (40°C)
0
2
4
6
8
Visible Charge [electrons (x10^5)]
3–94
7618A11

Figure 6:

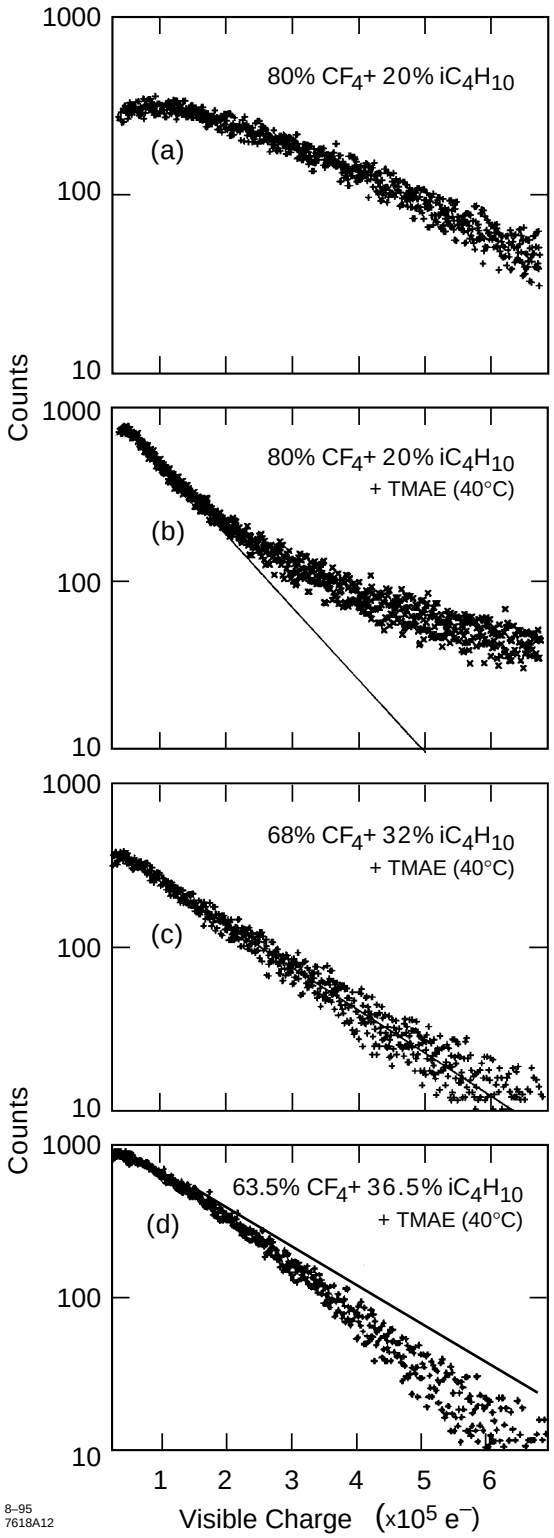
1000
100
10
80% CF_4+ 20% iC_4H_{10}
(a)
Counts
80% CF_4+ 20% iC_4H_{10}
+ TMAE (40°C)
(b)
68% CF_4+ 32% iC_4H_{10}
+ TMAE (40°C)
(c)
63.5% CF_4+ 36.5% iC_4H_{10}
+ TMAE (40°C)
(d)
1 2 3 4 5 6
Visible Charge (x10^5 e^-)
8–95
7618A12

Fig. 4

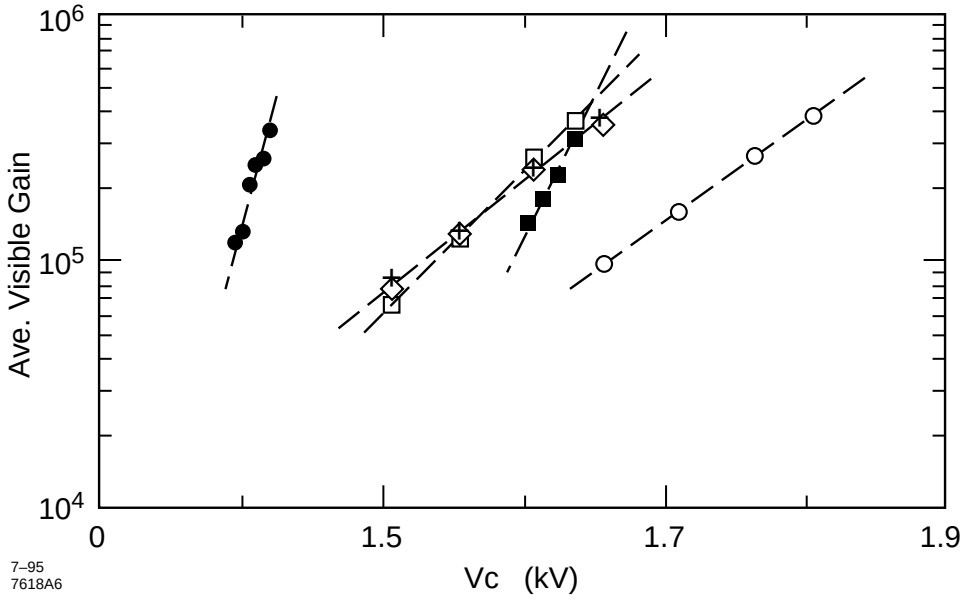

Figure 8:

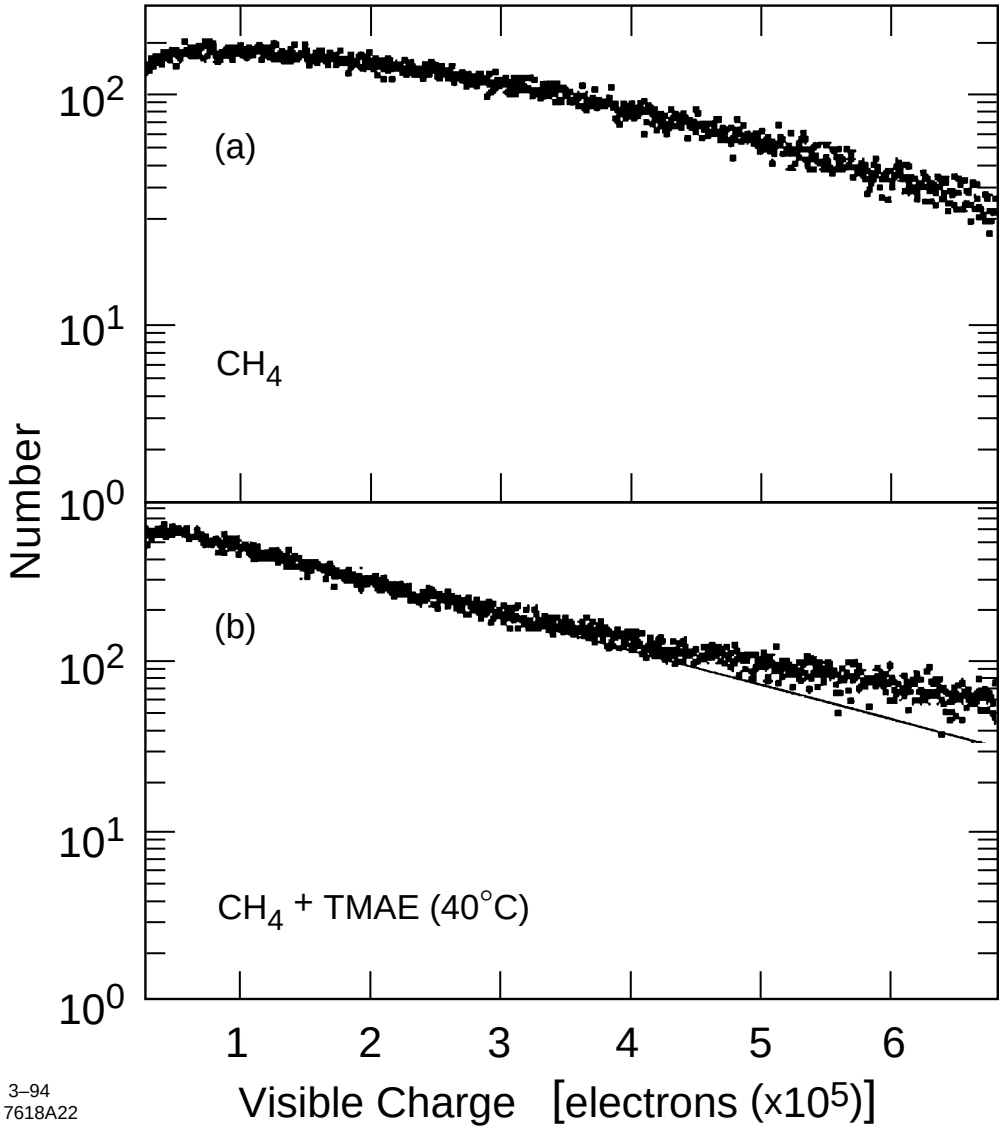
Number
10^2
10^1
10^0
(a)
CH_4
(b)
CH_4 + TMAE (40°C)
1
2
3
4
5
6
Visible Charge [electrons (x10^5)]
3–94
7618A22

Figure 9:

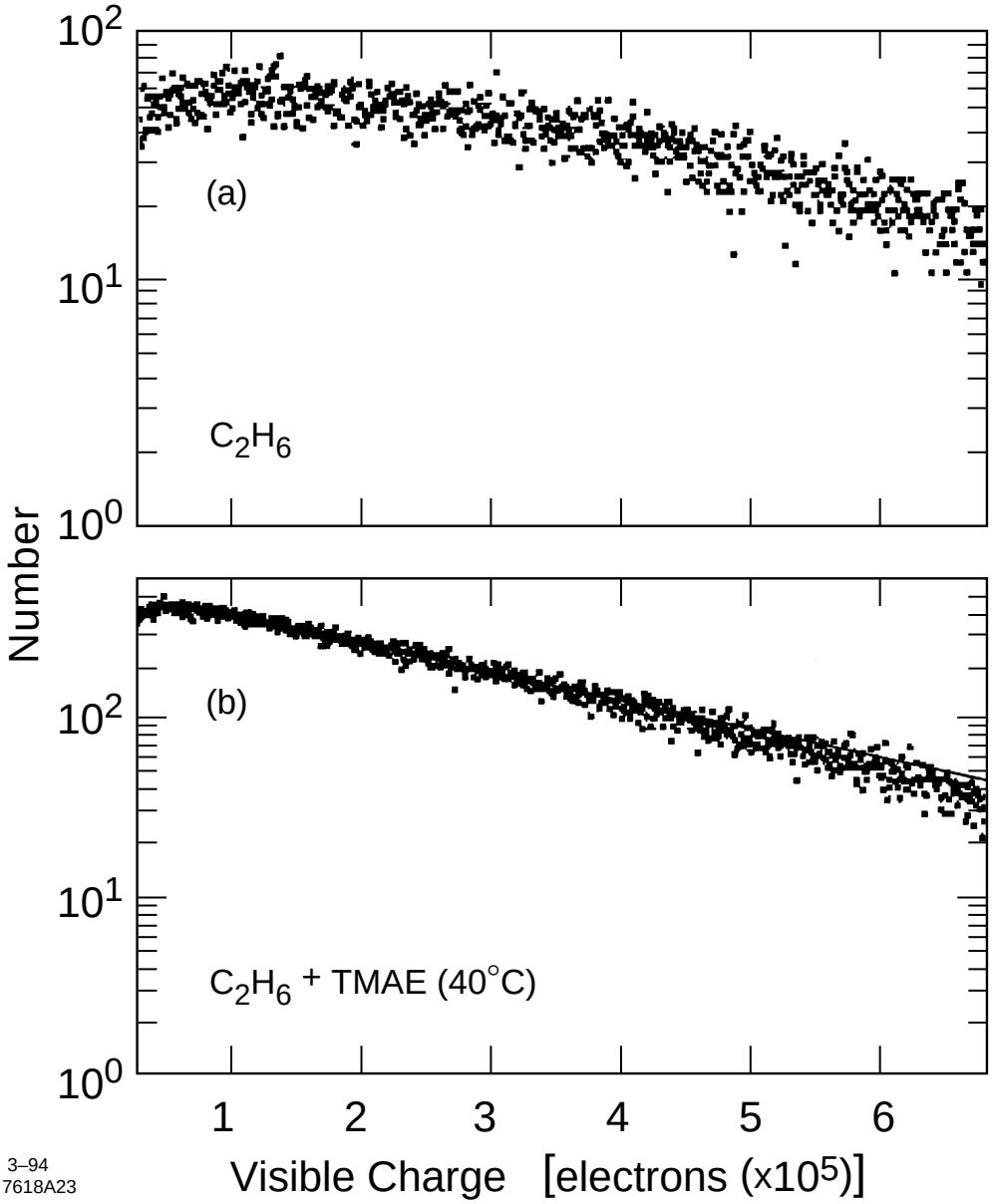
10^2
10^1
10^0
(a)
C_2H_6
Number
10^2
10^1
10^0
(b)
C_2H_6 + TMAE (40°C)
1
2
3
4
5
6
3–94
7618A23
Visible Charge [electrons (x10^5)]

Figure 11:

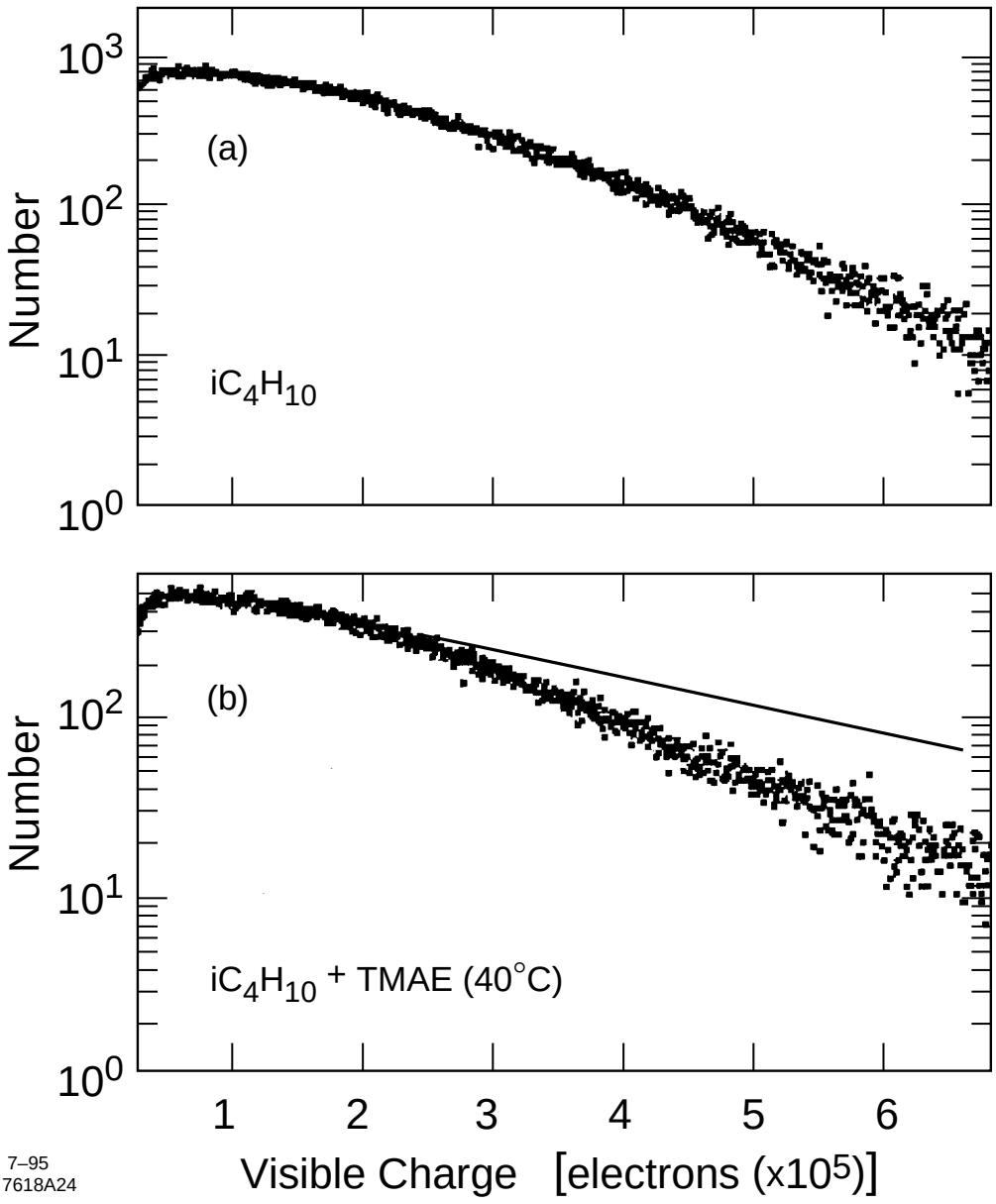
(a)
iC_4H_{10}
(b)
iC_4H_{10} + TMAE (40°C)
Number
Visible Charge [electrons (x10^5)]
7–95
7618A24

Figure 12:

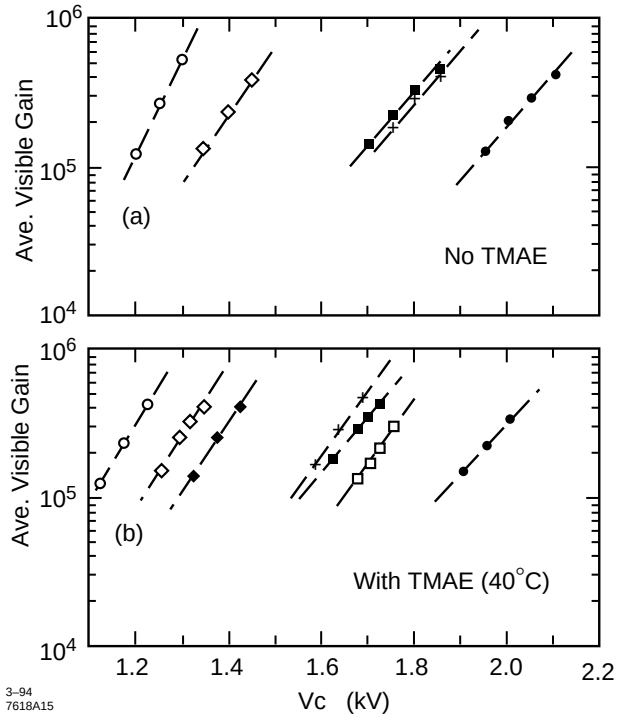
Ave. Visible Gain
10^6
10^5
10^4
(a)
No TMAE
Ave. Visible Gain
10^6
10^5
10^4
(b)
With TMAE (40°C)
1.2
1.4
1.6
1.8
2.0
2.2
Vc (kV)
3–94
7618A15

Figure 13:

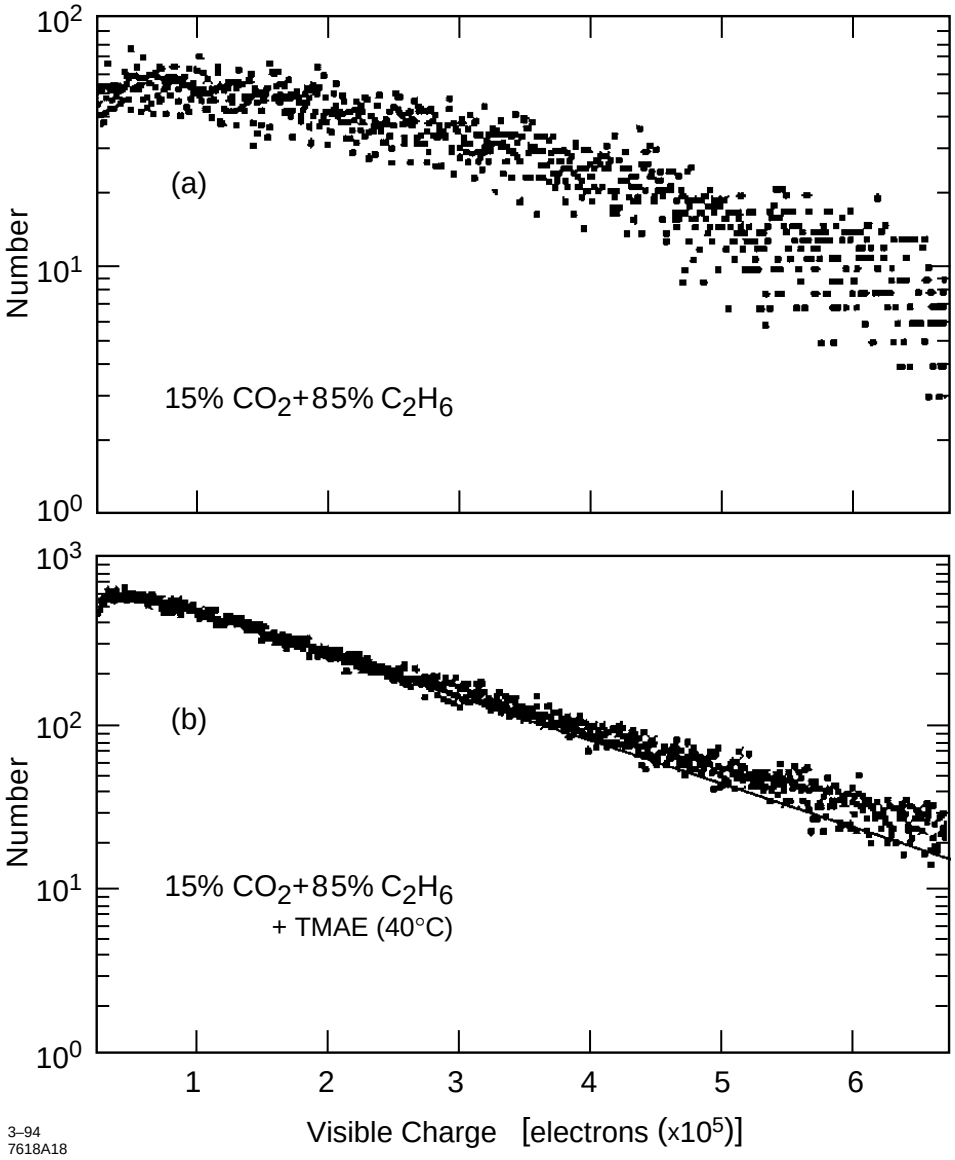
Number
(a)
15% CO2+85% C2H6
(b)
15% CO2+85% C2H6
+ TMAE (40°C)
Visible Charge [electrons (x10^5)]
3–94
7618A18

Figure 14:

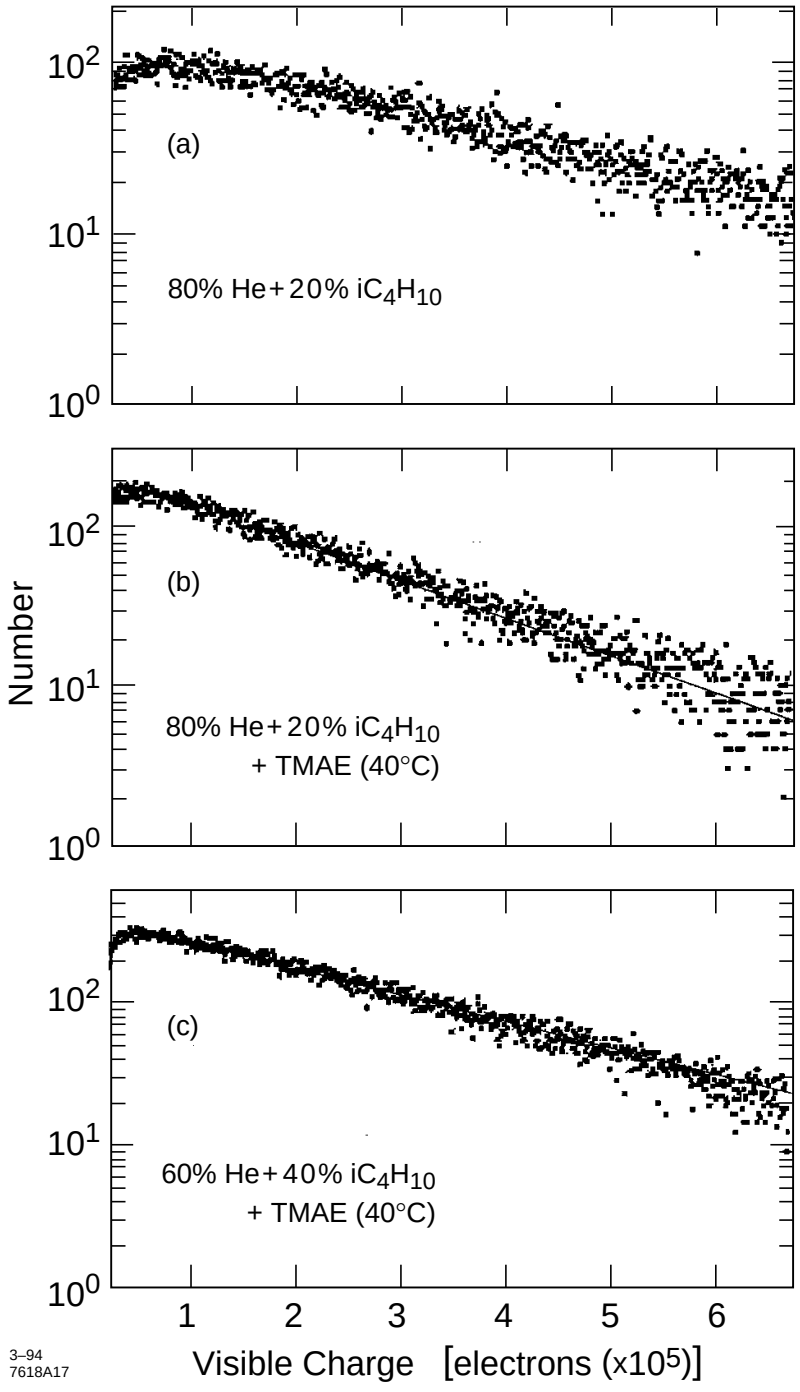
(a)
80% He + 20% iC4H10
(b)
80% He + 20% iC4H10
+ TMAE (40°C)
(c)
60% He + 40% iC4H10
+ TMAE (40°C)
Number
Visible Charge [electrons (x10^5)]
3–94
7618A17

Figure 15:

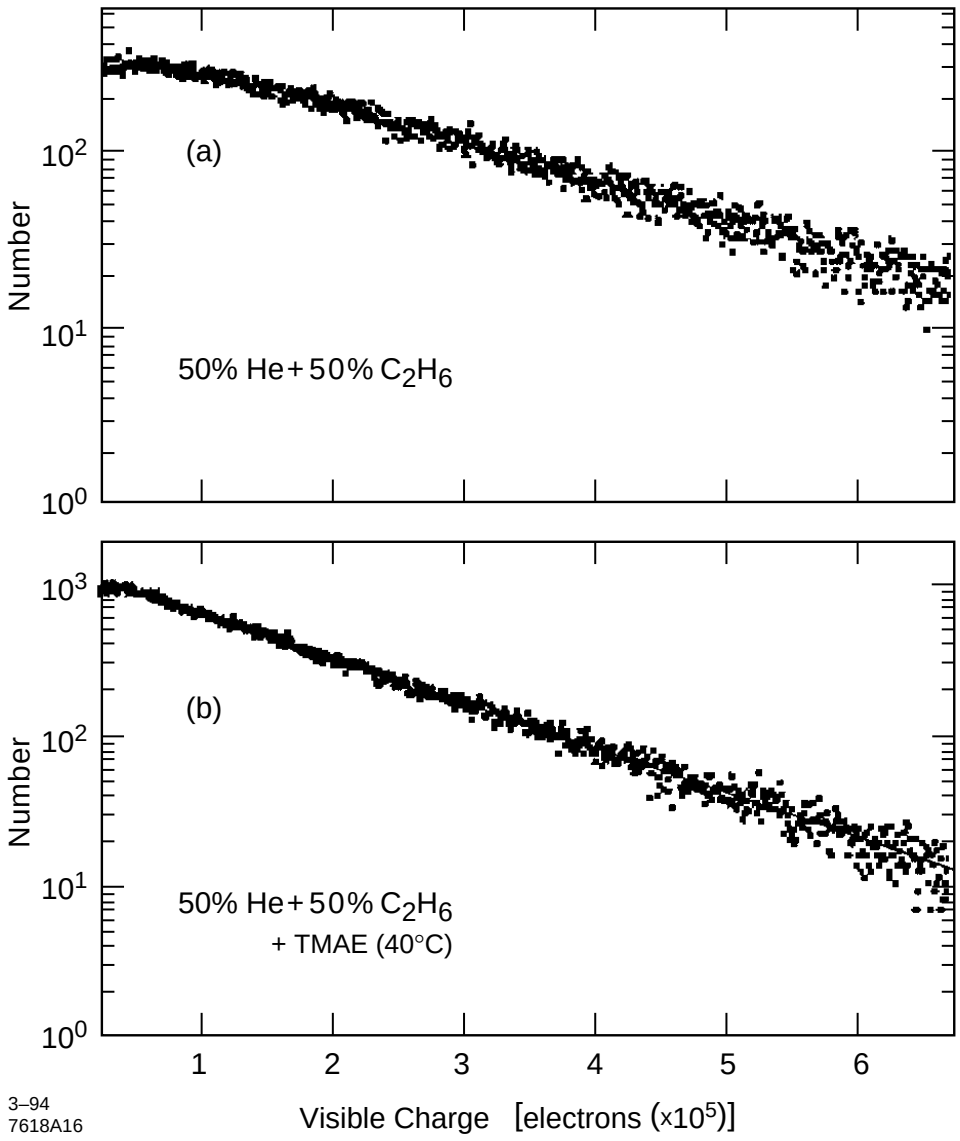
(a)
50% He + 50% C_2H_6
Number
10^2
10^1
10^0
(b)
50% He + 50% C_2H_6
+ TMAE (40°C)
Number
10^3
10^2
10^1
10^0
1
2
3
4
5
6
3–94
7618A16
Visible Charge [electrons (x10^5)]

Figure 16:

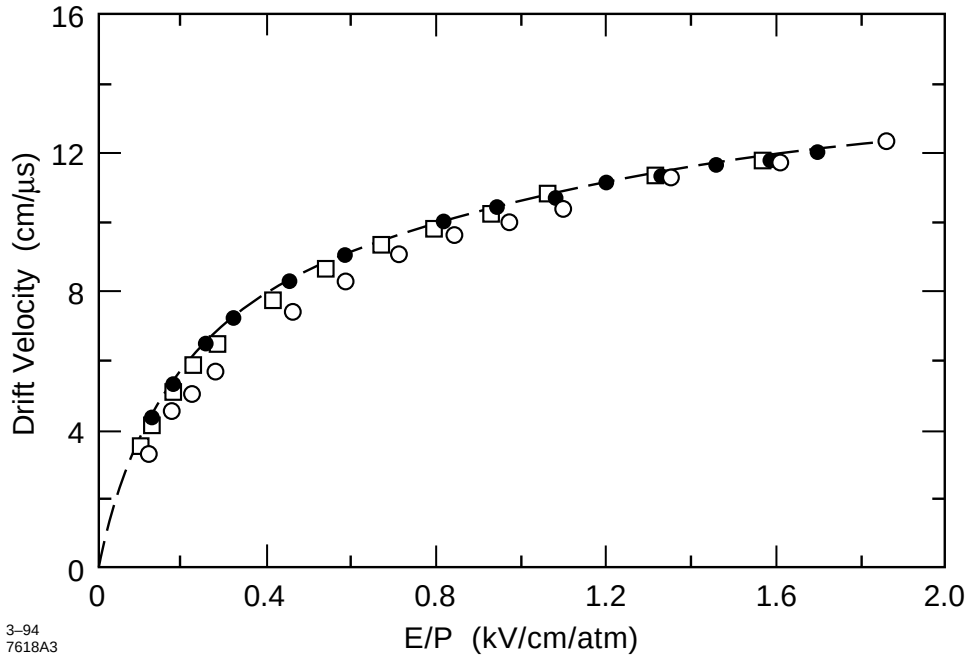

Figure 17:

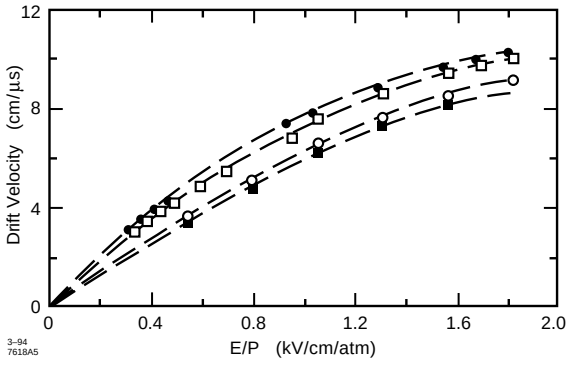

Figure 18:

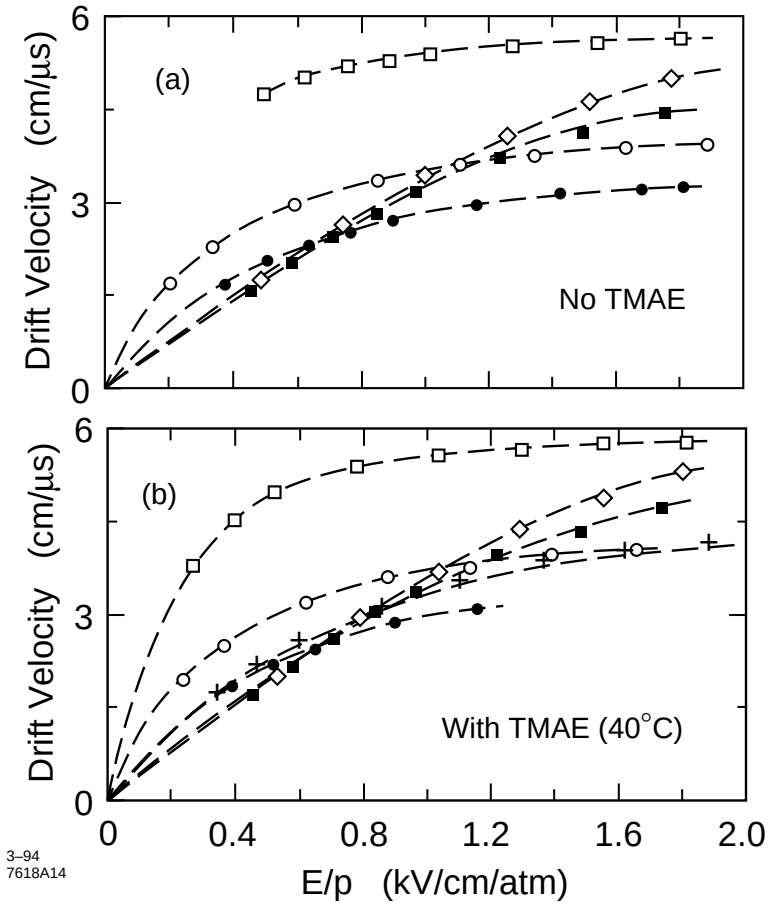
(a)
No TMAE
(b)
With TMAE (40°C)
Drift Velocity (cm/μs)
E/p (kV/cm/atm)
0
3
6
0.4
0.8
1.2
1.6
2.0
3–94
7618A14

Figure 19:

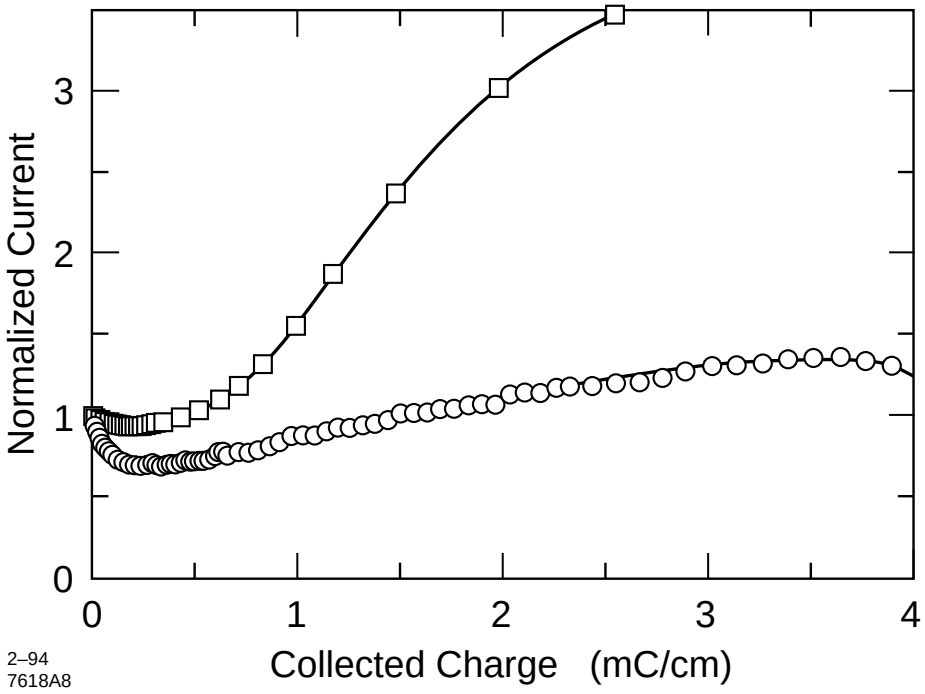
Normalized Current
0
1
2
3
0
1
2
3
4
Collected Charge (mC/cm)
2–94
7618A8

Figure 20:

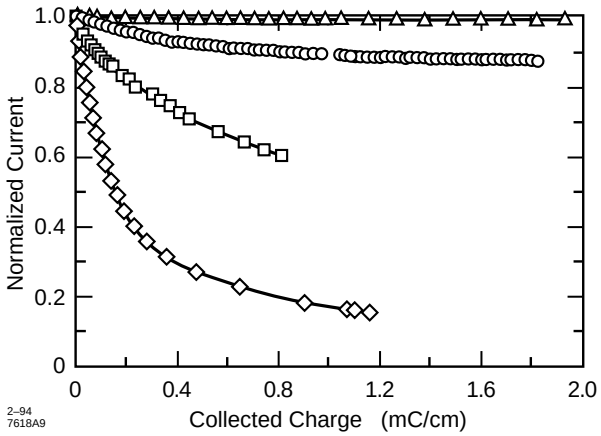

Fig. 6

Figure 21:

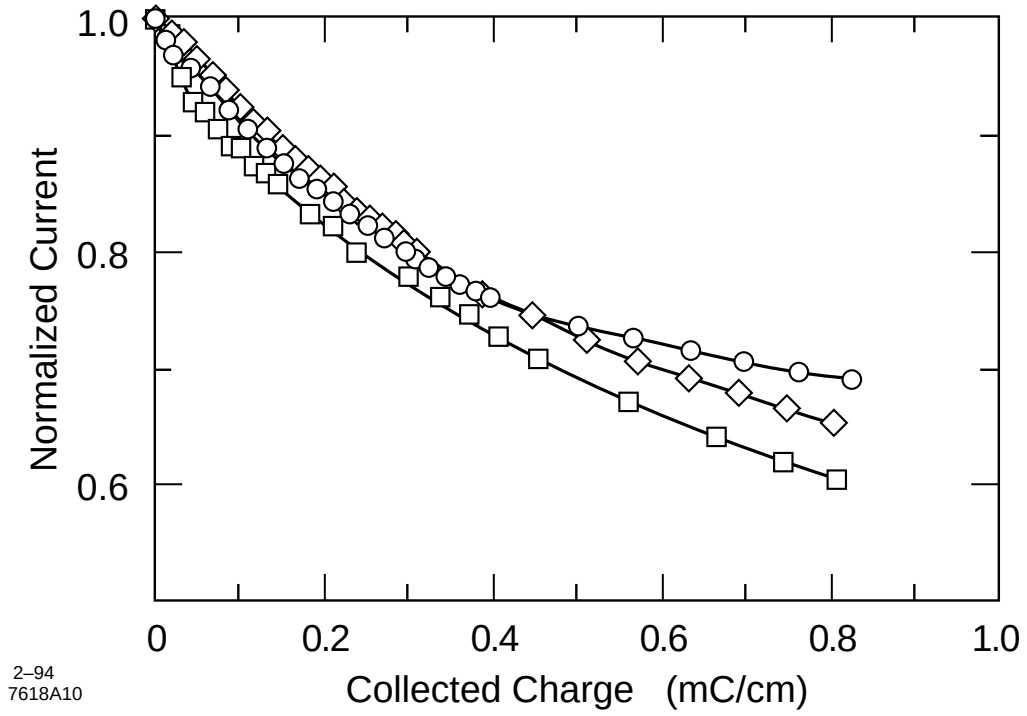
1.0
0.8
0.6
Normalized Current
0
0.2
0.4
0.6
0.8
1.0
Collected Charge (mC/cm)
2–94
7618A10

Figure 22: